Publicly available geosynchronous (GEO) space object catalog for future space situational awareness (SSA) studies

Darin C. Koblick
Joint PhD Candidate
California State University Long Beach and Claremont Graduate University

Praveen Shankar
Associate Professor
California State University Long Beach

Shujing Xu
Postdoctoral Scholar
University of California San Diego

Abstract

Previously, there have been many commercial proposals and extensive academic studies regarding ground and space based sensors to assist a space surveillance network in obtaining metric observations of satellites and debris near Geosynchronous Earth Orbit (GEO). Most use physics based models for geometric constraints, lighting, and tasker/scheduler operations of sensor architectures. Under similar physics modeling assumptions, the space object catalog is often different due to proprietary standards and datasets. Lack of catalog commonality between studies creates barriers and difficulty comparing performance benefits of sensor trades.

To solve this problem, we have constructed a future GEO space catalog from publicly available datasets and literature. The annual number of new payloads and rocket bodies is drawn from a Poisson distribution while the growth of the current GEO catalog is bootstrapped from the historical payload, upper stage, and debris data. We adopt a spherically symmetric explosion model and couple it with the NASA standard breakup model to simulate explosions of payloads and rocket bodies as they are the primary drivers of the debris population growth. The cumulative number of fragments follow a power-law distribution. Result from 1,000 random catalog growth simulations indicates that the GEO space object population in the year 2050 will include over 3,600 objects, nearly half of which are debris greater than 10 cm spherical diameter. The number of rocket bodies and dead payloads is projected to nearly double over the next 33 years. For comparison, the current Air Force Space Command catalog snapshot contains fewer than 50 pieces of debris and coarse Radar Cross Section (RCS) estimates which include: small, medium, and large. The current catalog may be sufficient for conjunction studies, but not for analyzing future sensor system performance. The 2050 GEO projected catalog will be available online for commercial/academic research and development.

1 Introduction

Since 1957 the United States Department of Defense (DoD) has maintained a catalog of space objects known as the Space Object Catalog (SATCAT). Satellite states (e.g., orbital elements) were improved upon with observations from the Space Surveillance Network (SSN) and recorded in two separate catalogs by the Air Force Space Command (AF-SPC) and by the Naval Space Command (NSC). Currently, the USSTRATCOM distributes the latest satellite catalog in the form of a SATCAT and two line element sets (TLEs) on `www.space-track.org`.

Maintaining an accurate space object catalog is important as it allows for increased situational awareness of threats to the North American continent as well as the US and Canadian interests in space [14]. SSA is the primary reason previous modeling and simulation campaigns help assess the performance of additional ground and space based sensors when working in conjunction with the SSN [4, 24, 7, 5]. This shows that it is important not only to have an accurate space object catalog but also to be able to predict the space environment in the future so we can wisely invest in R&D, new phenomenologies, and concept studies.

The scope of this research covers the assessment and projection of the current GEO space environment until the year 2050. Predicting the type, size, and quantity of satellites launched into GEO is fairly straightforward and can be based on the analysis of historical catalog data. However, predicting the debris environment is challenging. Debris is typically formed when a satellite breaks apart from a collision with another object or from an explosion. Both cases have been modeled using the NASA Standard Breakup Model [23, 20, 8] and typically involve predicting the quantity, mass, area, ejection velocity and direction of fragments generated after an on-orbit event.

The following sections below provide an overview of the process used to create our publicly available GEO space catalog from mining historical data for statistics to implementing an interpolation scheme between two fragment size distributions. Section two defines object types and orbit regimes, section three presents statistical analysis on historic data. Section four summarizes the modified NASA standard breakup model for GEO satellites and a linear interpolation model between two distinct size distributions, section five provides an overview of the catalog projection process and summarizes the results.

2 Satellite Object Types, Definitions, and Behavior

Currently, the satellite catalog (e.g., SATCAT) which is available from `http://www.space-track.org`, as well as `http://www.celestrak.com`, designates the following object types [13]:

Table 1: Object Type Definition

Nomenclature	**Short Description**
R/B	Rocket Body (can be either first stage or second stage)
DEB	Satellite debris may include tanks, lens covers, fragments, bolts, fairings, etc.
P/L	Satellite Payload that indicates that the object was intended to perform some type of mission. This can be further specified by describing its recent behavior as either an **Active Payload** or a **Dead Payload**. Note that **APL** and **DPL** will be used in our catalog to describe the payload status.

The JSpOC tracks satellites in four main orbital regimes which include: Low Earth Orbit (LEO), Medium Earth Orbit (MEO), Highly Elliptical Orbit (HEO), and Geosynchronous Earth Orbit (GEO) [9]. These regimes are defined by their orbital period, eccentricity, and inclination. For the purpose of this research, only the objects which fall into the GEO orbital regime definition will be considered.

Table 2: Orbit Regime Definition

Regime	**Period (P)**	**Eccentricity (e)**	**Inclination (i)**
LEO	$P < 225$ min	$e \geq 0$	any
HEO	$P \geq 225$ min	$e > 0.3$	any
MEO	$600 < P < 800$ min	$e \leq 0.3$	any
GEO	$1300 < P < 1800$ min	$e < 0.3$	$i < 35°$

Of the GEO orbital regime, we attempt to break down the category further by defining geosynchronous and geostationary satellites. Geostationary satellites remain over a specific latitude and longitude while the orbital period of geosynchronous satellites is matched to Earth's rotation rate [27]. In practice, a perfect match between the Earth's rotation and the satellite's orbital period is not possible due to the gravitational perturbations from Earth's gravity field, as well as the sun and the moon. East-West station keeping and sometimes, North-South station keeping may need to be performed for active payloads currently on or near the GEO belt.

Instead of incorporating controllers for all active GEO satellites, we recommend zeroing out their eccentricity and setting their semi-major axis to the value that matches the orbital period to Earth's rotation rate. A two-body propagator is recommended for active payloads so they do not start to drift over the duration of a mission simulation.

Dead payloads and rocket bodies are assumed to have been disposed of in accordance with the recommendations made by the Inter-Agency Space Debris Coordinate Committee (IADC) which call for 300 km or greater altitude above the GEO belt [10]. These objects are obviously not actively maintained and like debris, will drift about subject to the natural forces, such as solar radiation pressure, Earth's gravity gradients, and third body perturbations. For all satellites that are not designated as active payloads, we recommend using a high fidelity force model.

Consider INSAT-3A, a multipurpose communications satellite which was retired and moved into the graveyard orbit in 2016. The orbital elements obtained from N2YO are shown in Table 3.

Table 3: Perturbations Due to Gravitational Fields in GEO for INSAT-3A

a	e	i	ω	Ω	ν
42298.64007km	0.001585057	1.065549461°	236.1167253°	89.37921838°	86.34379872°

A high fidelity gravity model with the sun and moon perturbations was used to compare the change in orbital elements and geocentric position to that of a two-body solution [15]. This demonstrates both East-West drift (as noted by the change in Geocentric longitude), and North-South drifting.

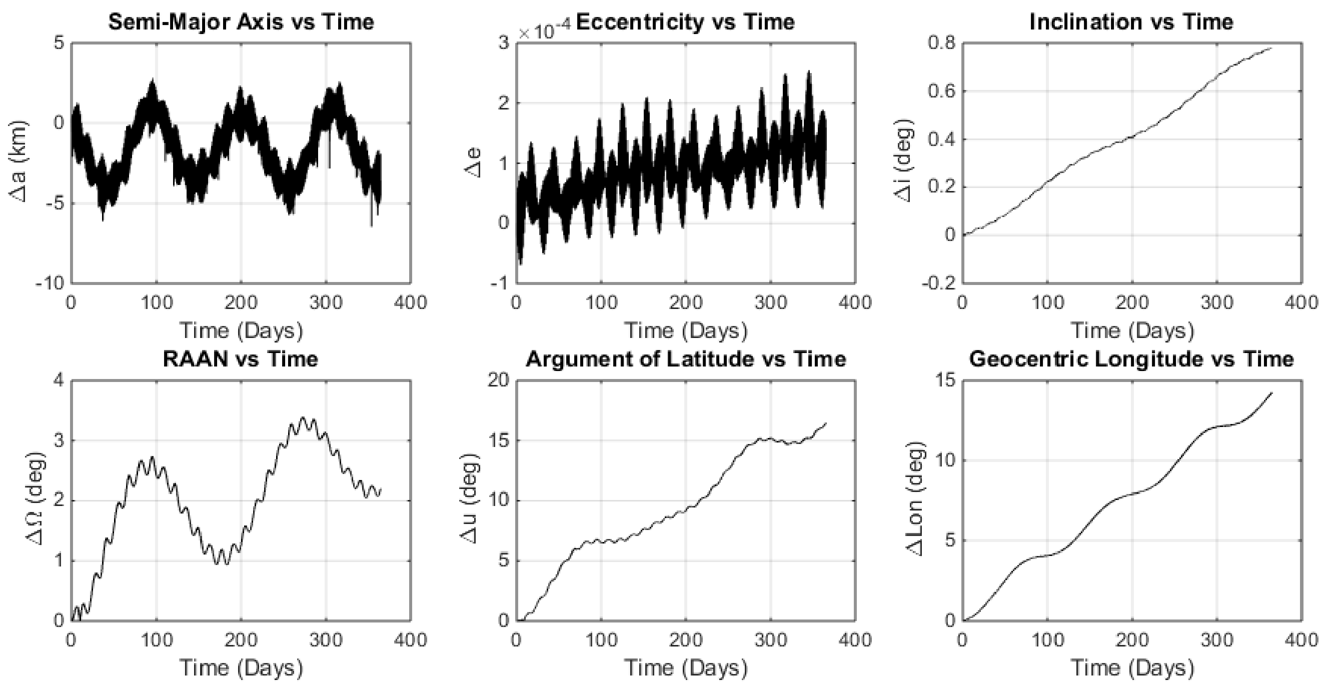

Fig. 1. Cataloged State Vector for INSAT-3A at 3/21/2017 00:00:00 UTC [25]

3 GEO Space Catalog Historical Data Analysis

A snapshot of the public satellite catalog obtained from Celestrak [13] and N2YO.com on March 21, 2017 was examined for the launch date, satellite type, and orbit regime. The active payload designation was found from cross correlating the NORAD catalog number with the Union of Concerned Scientists Satellite Database [6]. The Radar Cross Sections associated with each satellite were obtained from multiple public sources:

gsfc.nasa.gov NASA reports the object size estimates for certain satellites in the catalog.

NY2O.com A web based real-time satellite tracking tool website which contains TLE information from the AFSPC and other sources.

prismnet.com Has median RCS data for over 15,700 cataloged objects until the AFSPC discontinued its reporting of actual object size estimates in September of 2014.

astrogaurd Russian telescope catalog contains both RCS estimates and photometry on over 5,000 satellites.

The distribution of the obtained spherical diameter versus object type is shown in Fig. 2. Note that the majority of debris is below 0.5 meters while rocket bodies and payloads are distributed anywhere from several centimeters to 10 meters. This data is collected as a single measurement for the satellite at a specific orientation for a particular solar phase angle, resulting in a variation of size.

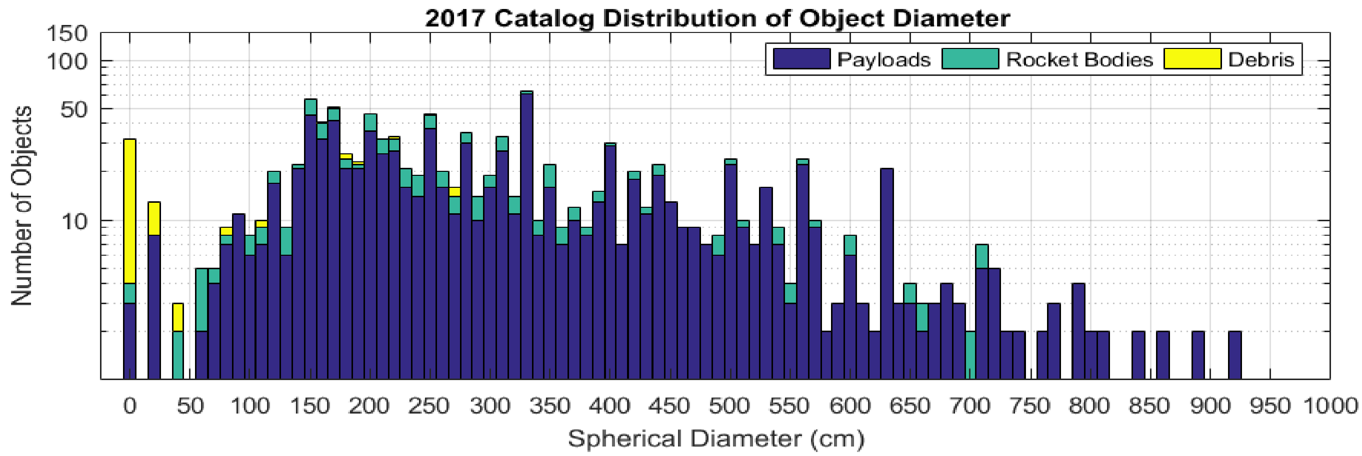

Fig. 2. 2017 Catalog Spherical Diameter Distribution by Object Type

Launch statistics of the number of payloads, number of rocket bodies, and number of debris fragments were examined over a 30-year time period (e.g., 1987–2017) and a Poisson fit was used to compute the average number of events per year (i.e., the arithmetic mean at a 95% fit confidence interval).

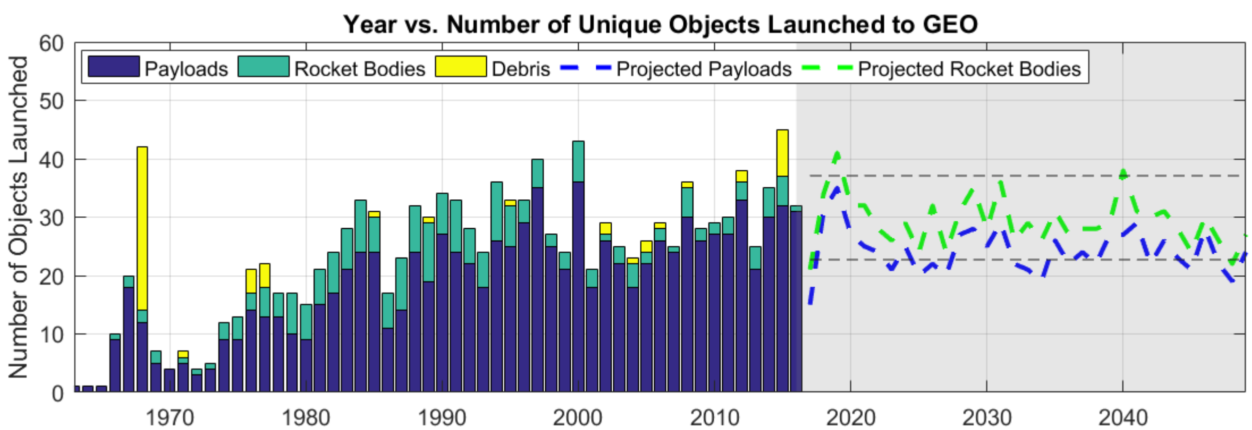

Fig. 3. Historical GEO Launch Data with Simulated Projections

Table 4: Annual Catalog Statistics by Launch Type (1987-2017)

Satellite Type	**mean (λ)**	**Standard Deviation (σ)**	**Annual Minimum**	**Annual Maximum**
Payloads	25.27	5.30	14	36
Rocket Bodies	4.63	2.74	1	10
Debris	0.63	1.54	0	8

While it may seem convenient to use a Gaussian distribution, a Poisson distribution is the defacto standard for statisticians when trying to express the probability of k number of events occurring over a fixed time interval. For reference, the probability of observing k events in an interval is

$$p(k \text{ events in interval}) = e^{-\lambda}\frac{\lambda^k}{k!}, \tag{1}$$

where λ is the average number of events per interval, and k is assumed to be nonnegative integers.

Explosions and on-orbit collisions are known sources of debris in lower Earth orbits. For GEO, previous research findings suggest that the number of collisions, which were likely to occur over the next hundred years, ranged from 0.2 to 0.4 suggesting that the only source of debris generation in GEO over the next three decades would be from explosions [18, 2].

Fragments from unknown explosions observed by NASA and ESA have led some to suggest that there should be 10 explosions to express the current GEO environment [11]. For modeling purposes, we will assume a 14.2% chance of either a rocket body or payload explosion per year. For a given satellite in GEO, the annual explosion rate of a payload has been reported to be 1.2×10^{-4} while rocket bodies have a slightly higher rate at 1.6×10^{-4} [2]. Looking at the average number of operational satellites and rocket bodies in GEO during the 100 year simulation, we estimate that the ratio of payloads explosions to rocket bodies is 4.2 to 10. Thus for every explosion that occurs, there is a 29.6% probability that it is a payload and a 70.4% likelihood of a rocket body.

4 Modified NASA Standard Breakup Model for GEO Satellites

Satellite and rocket body breakup models should define the size, area-to-mass ratio, and velocity imparted onto each fragment when modeling an event. The NASA standard breakup model is used when predicting the fragment size, area-mass ratio, and ΔV distributions [12, 19]. Fragments are typically predicted from a power law distribution,

$$N_{\text{cum}} = \text{sf} \times 6 \times L_c^{-1.6} \tag{2}$$

where N_{cum} is the cumulative number of fragments which are greater than the characteristic length L_c (in meters), and the scaling factor sf is found to be unity when the upper stages has a total mass between 600 and 1000 kg. For GEO, the scaling factor may vary between 0.7 and 3.8 depending on the satellite classification (e.g., rocket body or active satellite) [26].

Ejection velocities of explosion fragments are evaluated from on-orbit analysis and ground testing and its probability density of the normal distribution function, $f(\chi \mid \mu, \sigma) = \exp(-(\chi-\mu)^2/2\sigma^2))/\sqrt{2\pi\sigma^2}$, as shown below

$$D^{\text{EXP}}_{\Delta V} \sim N(\mu^{\text{EXP}}, \sigma^{\text{EXP}}, \log_{10}\Delta V^{\text{EXP}}); \tag{3}$$

where $\sigma^{\text{EXP}} = 0.4$, $\mu^{\text{EXP}} = 0.2\log_{10}\text{A/M} + 1.85$, and A/M is the area-to-mass ratio of the fragment. Previous literature has discussed how to model the area-to-mass distribution for both rocket body fragments and payloads [2, 12, 1].

For all explosion fragments with a characteristic length below 8 cm, including both rocket bodies (abbr. R/B) and payloads (abbr. P/L), a normal distribution function (derived from hypervelocity impact testing) can be used to estimate the area-to-mass ratio

$$D^{\text{small}}_{\text{A/M}}(\lambda_c, \chi) \sim N(\mu^{\text{small}}(\lambda_c), \sigma^{\text{small}}(\lambda_c) \mid \chi), \tag{4}$$

where $\lambda_c = \log_{10} L_c$, $\chi = \log_{10}$ A/M, and

$$\mu^{\text{small}} = \begin{cases} -0.3 & \lambda_c \le -1.75 \\ -0.3 - 1.4(\lambda_c + 1.75) & -1.75 < \lambda_c < -1.25 \\ -1.0 & \lambda_c \ge -1.25 \end{cases}, \quad \sigma^{\text{small}} = \begin{cases} 0.2 & \lambda_c \le -3.5 \\ 0.2 + 0.1333(\lambda_c + 3.5) & \lambda_c > -3.5 \end{cases}$$

For those fragments with a characteristic length larger than 11 cm, area-to-mass for rocket bodies (resp. payloads) follows a mixture model consisting of two normal distributions

$$D_{\text{A/M}}^{\text{R/B}}(\lambda_c, \chi) \sim \alpha^{\text{R/B}}(\lambda_c) N(\mu_1^{\text{R/B}}(\lambda_c), \sigma_1^{\text{R/B}}(\lambda_c) \mid \chi) + (1 - \alpha^{\text{R/B}}(\lambda_c)) N(\mu_2^{\text{R/B}}(\lambda_c), \sigma_2^{\text{R/B}}(\lambda_c) \mid \chi) \tag{5}$$

$$D_{\text{A/M}}^{\text{P/L}}(\lambda_c, \chi) \sim \alpha^{\text{P/L}}(\lambda_c) N(\mu_1^{\text{P/L}}(\lambda_c), \sigma_1^{\text{P/L}}(\lambda_c) \mid \chi) + (1 - \alpha^{\text{P/L}}(\lambda_c)) N(\mu_2^{\text{P/L}}(\lambda_c), \sigma_2^{\text{P/L}}(\lambda_c) \mid \chi) \tag{6}$$

where

$$\alpha^{\text{R/B}} = \begin{cases} 1.0 & \lambda_c \leq -1.4 \\ 1.0 - 0.3571(\lambda_c + 1.4) & -1.4 < \lambda_c < 0 \\ 0.5 & \lambda_c \geq 0 \end{cases}, \quad \alpha^{\text{P/L}} = \begin{cases} 0 & \lambda_c \leq -1.95 \\ 0.3 - 0.4(\lambda_c + 1.2) & -1.95 < \lambda_c < 0.55 \\ 1.0 & \lambda_c \geq 0.55 \end{cases}$$

$$\mu_1^{\text{R/B}} = \begin{cases} -0.45 & \lambda_c \leq -0.5 \\ -0.45 - 0.9(\lambda_c + 0.5) & -0.5 < \lambda_c < 0 \\ -0.9 & \lambda_c \geq 0 \end{cases}, \quad \mu_1^{\text{P/L}} = \begin{cases} -0.6 & \lambda_c \leq -1.1 \\ -0.6 - 0.318(\lambda_c + 1.1) & -1.1 < \lambda_c < 0 \\ -0.95 & \lambda_c \geq 0 \end{cases}$$

$$\sigma_1^{\text{R/B}} = 0.55, \quad \sigma_1^{\text{P/L}} = \begin{cases} 0.1 & \lambda_c \leq -1.3 \\ 0.1 - 0.2(\lambda_c + 1.3) & -1.3 < \lambda_c < 0.3 \\ 0.3 & \lambda_c \geq -0.1 \end{cases}$$

$$\mu_2^{\text{R/B}} = -0.9, \quad \mu_2^{\text{P/L}} = \begin{cases} -1.2 & \lambda_c \leq -0.7 \\ -1.2 - 1.333(\lambda_c + 0.7) & -0.7 < \lambda_c < -0.1 \\ -2.0 & \lambda_c \geq -0.1 \end{cases}$$

$$\sigma_2^{\text{R/B}} = \begin{cases} 0.28 & \lambda_c \leq -1.0 \\ 0.28 - 0.1636(\lambda_c + 1) & -1 < \lambda_c < 0.1 \\ 0.1 & \lambda_c \geq 0.1 \end{cases}, \quad \sigma_2^{\text{P/L}} = \begin{cases} 0.5 & \lambda_c \leq -0.5 \\ 0.5 - (\lambda_c + 0.5) & -0.5 < \lambda_c < -0.3 \\ 0.3 & \lambda_c \geq -0.3 \end{cases}$$

A probability distribution function for fragments between 8 cm and 11 cm is not available so one dimensional linear interpolation is performed between the distribution function for small fragments (Equation 4) and large fragments (Equations 5–6) [3]. Letting the characteristic length be the interpolation parameter we define the interpolation coordinate β as

$$\beta = \frac{L_c - L_c^{8\text{cm}}}{L_c^{11\text{cm}} - L_c^{8\text{cm}}} = \frac{L_c - 0.08}{0.03} = \frac{10^{\lambda_c} - 0.08}{0.03} \tag{7}$$

where $L_c \in (0.08, 0.11)$ m, $L_c^{8\text{cm}} = 0.08$, and $L_c^{11\text{cm}} = 0.11$. The means of the distributions, $\mu^{8\text{cm}}$, $\mu_1^{11\text{cm}}$ and $\mu_2^{11\text{cm}}$ corresponding to $L_c^{8\text{cm}}$ and $L_c^{11\text{cm}}$, and the interpolated mean corresponding to L_c can be obtained for both rocket bodies and payloads from $\mu_i = (1 - \beta)\mu^{8\text{cm}} + \beta\mu^{11\text{cm}}$:

$$\begin{aligned} \mu_{1i}^{\text{R/B}} &= 0.55\beta - 1 && (8) \\ \mu_{1i}^{\text{P/L}} &= 1.1683\beta - 1 && (9) \\ \mu_{2i}^{\text{R/B}} &= 0.1\beta - 1 && (10) \\ \mu_{2i}^{\text{P/L}} &= -0.2\beta - 1 && (11) \end{aligned}$$

Using the same interpolation parameter as used for the mean in Equation 7, the standard deviation is found for both rocket bodies and payloads for fragment characteristic lengths between 8 cm and 11 cm from

$$\sigma = \sqrt{(1 - \beta)(\sigma^{8\text{cm}})^2 + \beta(\sigma^{11\text{cm}})^2}$$

such that

$$\begin{aligned} \sigma_{1i}^{\text{R/B}} &= \sqrt{0.2707 + 0.0318\beta} && (12) \\ \sigma_{1i}^{\text{P/L}} &= \sqrt{0.2707 - 0.2424\beta} && (13) \\ \sigma_{2i}^{\text{R/B}} &= \sqrt{0.2707 - 0.1923\beta} && (14) \\ \sigma_{2i}^{\text{P/L}} &= \sqrt{0.2707 - 0.0207\beta} && (15) \end{aligned}$$

The parameters in Equations 8 –15 may be substituted into the mixture model described by Equation 5 and 6 resulting in an area-to-mass ratio that can be computed for those fragments between 8 cm and 11 cm from Equations 16 and 17.

$$D^{i\text{R/B}}_{\text{A/M}}(\lambda_c,\chi) \;=\; \alpha^{\text{R/B}}(\lambda_c)N(\mu^{\text{R/B}}_{1i}(\lambda_c),\sigma^{\text{R/B}}_{1i}(\lambda_c)\mid\chi)+(1-\alpha^{\text{R/B}}(\lambda_c))N(\mu^{\text{R/B}}_{2i}(\lambda_c),\sigma^{\text{R/B}}_{2i}(\lambda_c)\mid\chi) \tag{16}$$

$$D^{i\text{P/L}}_{\text{A/M}}(\lambda_c,\chi) \;=\; \alpha^{\text{P/L}}(\lambda_c)N(\mu^{\text{P/L}}_{1i}(\lambda_c),\sigma^{\text{P/L}}_{1i}(\lambda_c)\mid\chi)+(1-\alpha^{\text{P/L}}(\lambda_c))N(\mu^{\text{P/L}}_{2i}(\lambda_c),\sigma^{\text{P/L}}_{2i}(\lambda_c)\mid\chi) \tag{17}$$

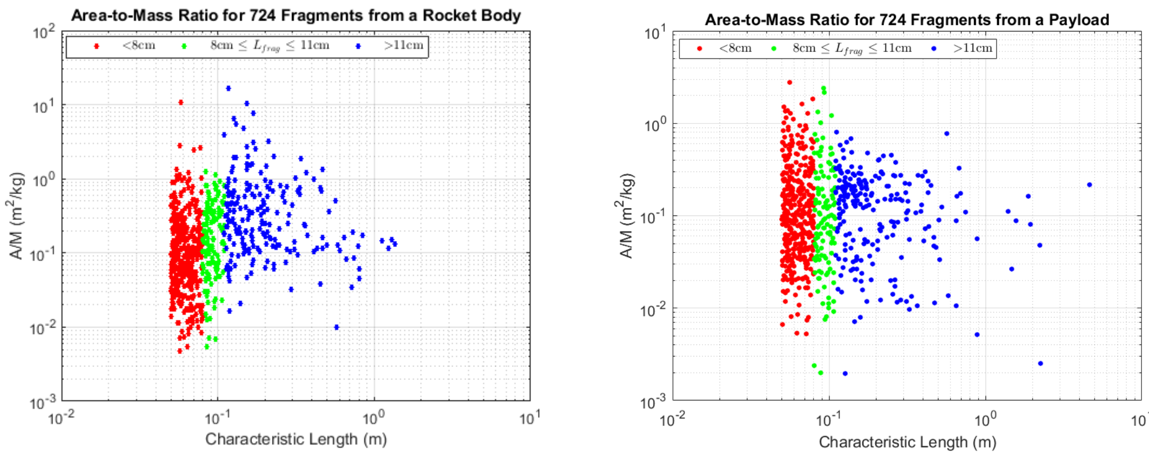

Fig. 4. Area-to-Mass Ratio vs Characteristic Length for Explosion Fragments between 5 cm and 10 m for both rocket bodies (left) and payloads (right)

The averaged cross-sectional area, A_x^{EXP}, in m^2 is found from the characteristic length of each fragment [12]

$$\begin{aligned} A_x^{\text{EXP}} &= 0.540424L_c^2, & L_c &< 0.00167\text{m} \\ A_x^{\text{EXP}} &= 0.556945L_c^{2.0047077}, & L_c &\geq 0.00167\text{m} \end{aligned}$$

The corresponding explosion fragment mass, M^{EXP}, can be determined by the reverse ratio of area-to-mass,

$$M^{\text{EXP}} = A_x^{\text{EXP}}/(\text{A/M}) \tag{18}$$

The corresponding distribution of ejection velocities for both rocket bodies and payloads is shown in Fig. 5 while the distribution of the averaged cross-sectional area is displayed in Fig. 6. Note that the ejection velocity distribution of the rocket body appears to follow the composite distribution for over 1400 fragments from the Delta, Ariane, and Cosmos upper stages as depicted in EVOLVE 4.0 [12].

From previous studies, it is assumed that when a satellite or rocket body explosion fragments follow a spherically symmetric distribution of increased velocity, ΔV, from the position vector, r_0 at which it occurred[28]. Unless specific geometries and materials about a satellite are known a priori, there is an equal likelihood that the velocity direction imparted onto a fragment will land anywhere on a unit sphere. The velocity direction of each fragment can be found from sphere point picking [21]

$$\begin{bmatrix}\dot{x}\\ \dot{y}\\ \dot{z}\end{bmatrix} = \left\|\Delta V^{\text{EXP}}\right\| \begin{bmatrix} 2x_1\sqrt{1-x_1^2-x_2^2} \\ 2x_2\sqrt{1-x_1^2-x_2^2} \\ 1-2(x_1^2+x_2^2)\end{bmatrix}, \tag{19}$$

where both x_1 and x_2 are drawn from a uniform distribution on $(-1,+1)$ on a unit circle, i.e., $x_1^2+x_2^2<1$.

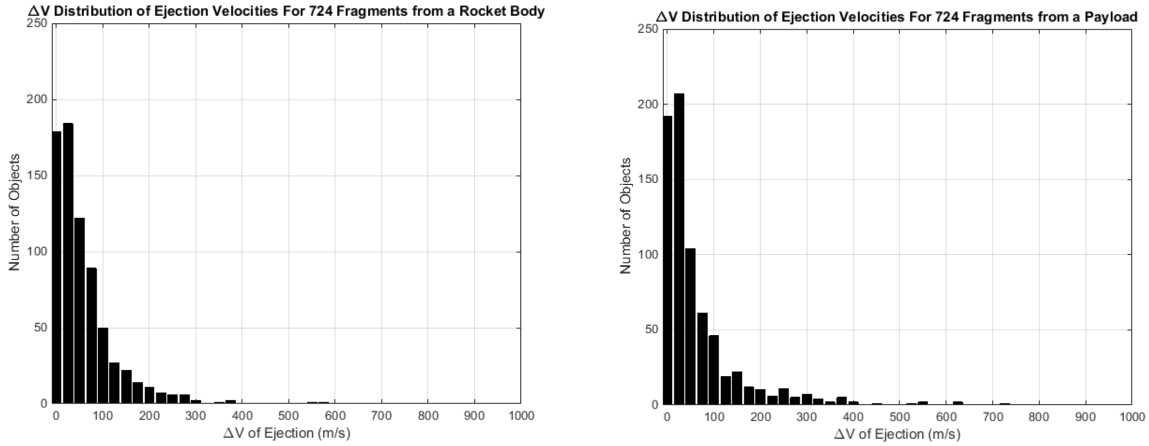

Fig. 5. Ejection Velocity Distributions for Explosion Fragments between 5 cm and 10 m for both rocket bodies (left) and payloads (right)

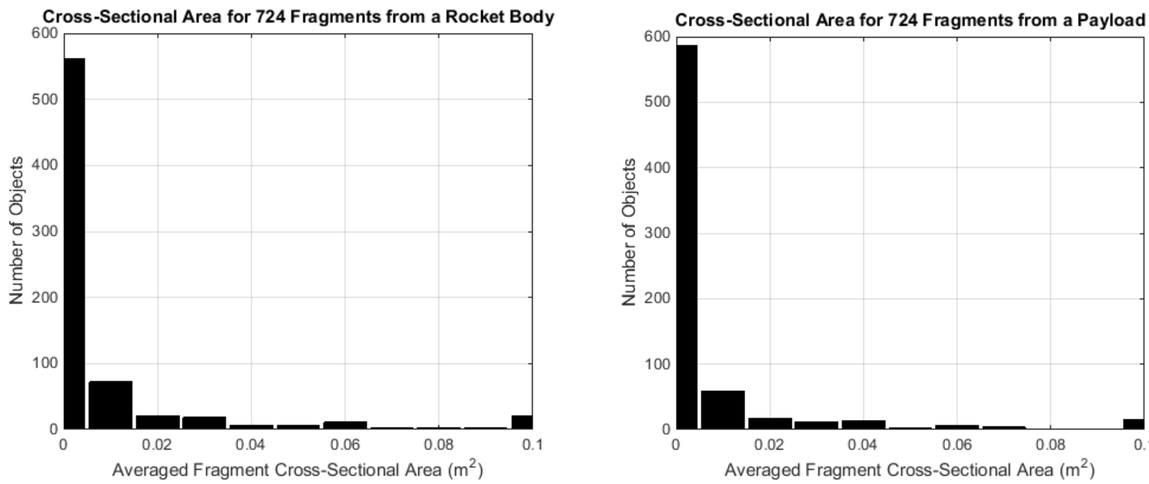

Fig. 6. Cross Sectional Area Distribution for Explosion Fragments between 5 cm and 10 m for both rocket bodies

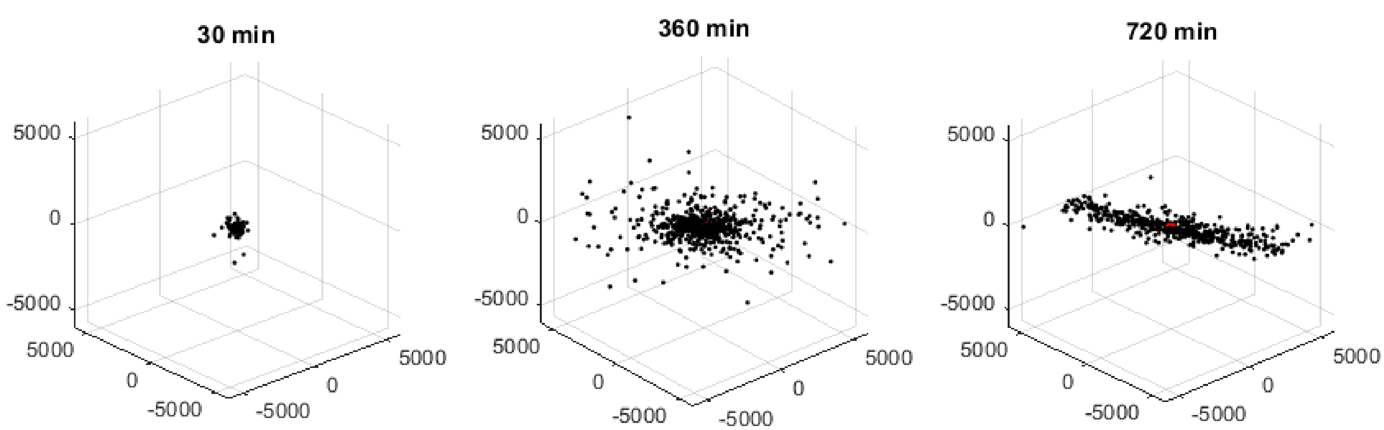

Fig. 7. Propagated Debris Fragments (5cm to 10m) After Rocket Body Explosion (distance in km from the parent object)

5 GEO Space Catalog Projection Process

The process of constructing a future GEO space catalog is depicted in Fig. 8. Given N number of years from 2017, for each year, the total number of dead payloads, rocket bodies, and debris is determined from the average number of events per year in Table 4 following the Poisson distribution in Equation 1. Once the number of each quantity is known, a uniform random sample of both orbital elements and radar cross section values is obtained from the initial satellite population fore each category. We assume that the number of active payloads in GEO will stay roughly the same such that any new GEO payloads will be treated as dead payloads and put into graveyard orbit.

As discussed in section 3, there is roughly a 14.2% likelihood of a rocket body or payload explosion per year. To simulate this, a uniform random number is generated on $[0, 1]$ and compared against this probability. If the random number is less than or equal to the likelihood of an on-orbit explosion, we perform another random draw to determine if the explosion was a rocket body or a payload. The NASA breakup model outlined in section 4 is used with the scaling factor in Equation 2 set to unity if the explosion occurred on a rocket body, otherwise another random draw is performed on the interval $[0.7, 3.8]$ if the satellite were a payload. The new explosion fragments, based on the minimum characteristic length (in this case $L_{\min} = 10$ cm), are added to the future GEO catalog and the exploded object is then removed. The explosion fragments are propagated forward from the current year of the explosion until the last year of the catalog projection, their positions and velocities are frozen in an Earth Centered Earth Fixed coordinate frame (ECEF) and the Epoch is set to that of the initial 2017 satellite population at which point the ECEF coordinates are converted back to an Earth Centered Inertial (ECI) coordinate frame.

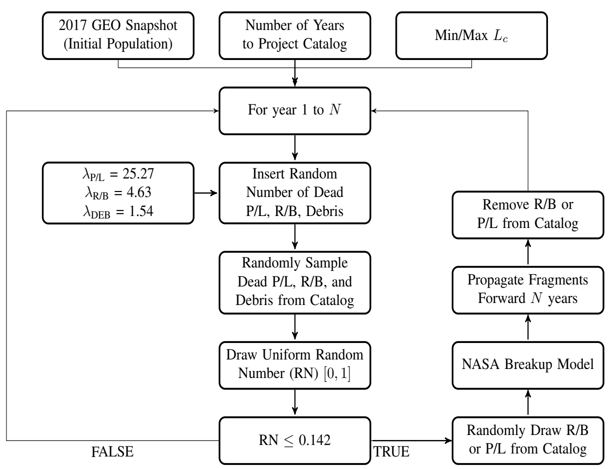

Fig. 8. Diagram of GEO Catalog Projection Process

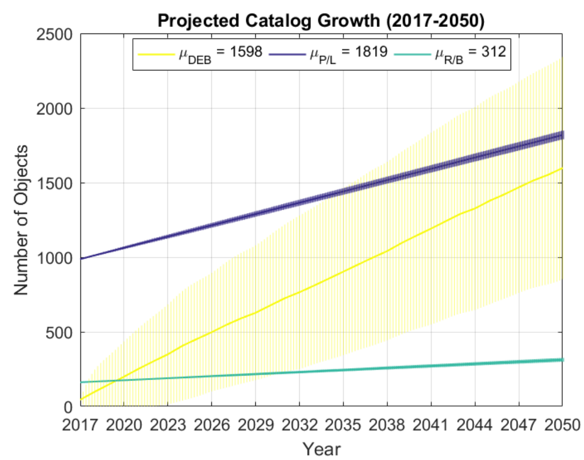

Fig. 9. Projected Growth in GEO Regime Until the Year 2050 with Explosion Fragments 10cm or larger

Using the catalog projection process (depicted in Fig. 8), we ran one thousand random trials and provided a summary of the results in Fig. 9. As expected, the variance about payload growth (including both dead and active) and rocket body growth is small compared to the number of explosion fragments over the next 33 years due to varying object size and type of the parent. The standard deviation for each category is overlaid on the average number of objects in Fig. 9. For simulation purposes, a representative catalog containing a near average number of objects in each category is selected. The growth of this catalog is depicted in Fig. 10 along with a comparison with today's catalog data. This catalog is made available online `www.Astro-Sciences.com` in Microsoft Excel format as shown in Fig. 11.

Our representative projected 2050 GEO catalog has a total of 3,696 objects ranging in diameter from 6 cm to over 22 m. We used the J2000 ECI reference frame with a March 21, 2017 00:00:00 common epoch (provided in Julian days). Object types were provided as debris (DEB), rocket bodies (R/B), active payloads (AP/L), and dead payloads (DP/L) along with their corresponding Radar Cross Sectional areas in square meters. This catalog represents the average of all random trials performed which should be a good "business as usual" case to use for most architecture and space systems modeling and simulation mission campaigns.

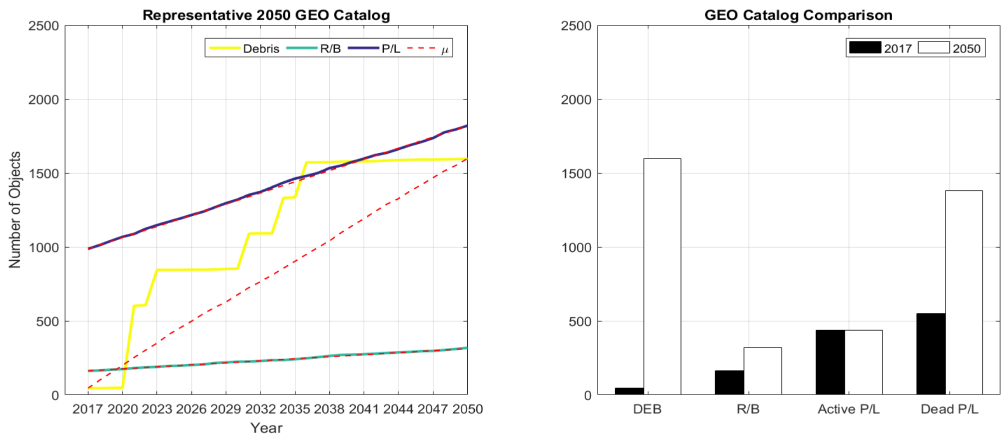

Fig. 10. Representative GEO Catalog Projection and Comparison with 2017 Historical Data

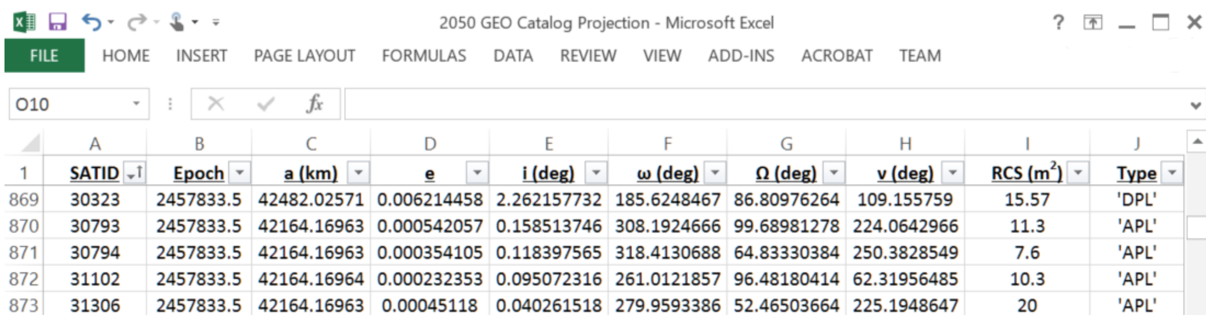

	A	B	C	D	E	F	G	H	I	J
1	SATID	Epoch	a (km)	e	i (deg)	ω (deg)	Ω (deg)	ν (deg)	RCS (m²)	Type
869	30323	2457833.5	42482.02571	0.006214458	2.262157732	185.6248467	86.80976264	109.155759	15.57	'DPL'
870	30793	2457833.5	42164.16963	0.000542057	0.158513746	308.1924666	99.68981278	224.0642966	11.3	'APL'
871	30794	2457833.5	42164.16963	0.000354105	0.118397565	318.4130688	64.83330384	250.3828549	7.6	'APL'
872	31102	2457833.5	42164.16964	0.000232353	0.095072316	261.0121857	96.48180414	62.31956485	10.3	'APL'
873	31306	2457833.5	42164.16963	0.00045118	0.040261518	279.9593386	52.46503664	225.1948647	20	'APL'

Fig. 11. Screenshot of a Sample 2050 Catalog Data in Microsoft Excel

While this catalog contains reasonable projections for the satellite state vectors, types, and size estimates choosing the correct propagation techniques, initial uncertainties (e.g., covariance), and illumination models are critical in order to producing meaningful results.

6 Conclusions & Future Work

We have outlined the necessary steps to arrive at an average representation of an object catalog for the GEO environment in the year 2050. These steps include historical analysis of rocket launches, payload deployments, and debris formation in GEO. We found that the primary driver for growth (and also the largest variance) was explosion fragments from rocket bodies and payloads, followed by dead payloads and rocket bodies. The NASA standard breakup model for GEO satellites was used and a method to interpolate between small and large fragment sizes was developed in order to bridge the gap between 8 cm and 11 cm fragment sizes.

Future work will include expanding the catalog to cover additional orbital regimes. Currently we have provided a realistic projection of the GEO space environment over the next three decades, but for full architecture analysis activities projections are needed for LEO, MEO, and HEO regimes. As of 2013 there were an estimated 22,000 objects in orbit (including thousands of tracks on objects that cannot be correlated), by the year of 2030 this number is projected to triple [16, 17].

References

[1] Anz-Meador, P. D. and Matney, M. J., *An assessment of the nasa explosion fragmentation model to 1 mm characteristic sizes*, Advances in Space Research, 34(5):987–992, 2004.

[2] Ariyoshi, Y. and Hanada, T., *Geodeem 4.0: Updated model for better understanding geo debris environment*, 2009.

[3] Bursal, F. H., *On interpolating between probability distributions*, Applied Mathematics and Computation, 77(2):213–244, 1996.

[4] Butkus, A. et al, *Space surveillance network and analysis model (ssnam) performance improvements*, 2007.

[5] Du, H. et al, *An/fsy-3 space fence system support of conjunction assessment michael g. koltiska, 2d lt*, 2016.

[6] Grimwood, T., *Ucs satellite database*, Union of Concerned Scientists, 31, 2017.

[7] Hall, R. and Johnson, T., *Commercial ssa catalog performance*, 2016.

[8] Hanada, T. et al, *Using NASA standard breakup model to describe low-velocity impacts on spacecraft*, Journal of spacecraft and rockets, 42(5):859–864, 2005.

[9] Hejduk, M. D. and Ghrist, R. W., *Solar radiation pressure binning for the geosynchronous orbit*, 2011.

[10] IADC Steering Group and others, *Space debris: Iadc assessment report for 2011*, 2011.

[11] Johnson, N. L., *Evidence for historical satellite fragmentations in and near the geosynchronous regime*, 2001.

[12] Johnson, N. L. and Krisko, P. H. and Liou, J. C. and Anz-Meador, P. D., *NASA's new breakup model of evolve 4.0*, Advances in Space Research, 28(9):1377–1384, 2001.

[13] Kelso, T. S., *Celestrak*, Public Domain Satellite Tracking Data, 2017.

[14] Kelso, T. S., *Space surveillance*, Celestrak, URL `https://celestrak.com/columns/v04n01/[cited08July2017]`, 2017.

[15] Koblick, D. et al, *Parallel high-precision orbit propagation using the modified picard-chebyshev method*, 2012.

[16] Lele, A., *Space awareness: A need for a multilateral mechanism*, Strategic Analysis, 37(5):610–620, 2013.

[17] Leonard, D., *Ugly truth of space junk: Orbital debris problem to triple by 2030*, Space.com, 2011.

[18] Liou, J. C., *Collision activities in the future orbital debris environment*, Advances in Space Research, 38(9):2102–2106, 2006.

[19] Liou, J. C., *Orbital debris modeling*, 2012.

[20] Liou, J. C. et al, *LEGEND–a three-dimensional LEO-to-GEO debris evolutionary model*, Advances in Space Research, 34(5):981–986, 2004.

[21] Marsaglia, G., *Choosing a point from the surface of a sphere*, The Annals of Mathematical Statistics, 43(2):645–646, 1972.

[22] Reynolds, R. C., *Review of current activities to model and measure the orbital debris environment in low-earth orbit*, Advances in Space Research, 10(3-4):359–371, 1990.

[23] Reynolds, R. C. et al, *NASA standard breakup model 1998 revision*, Lockheed Martin Space Operations Report LMSMSS-32532, Houston, TX, 1998.

[24] Shick, B., *Expanding lookout capabilities for architectural analysis*, 2009.

[25] Tracking, Real-Time Satellite, *N2yo*, 2017.

[26] Uetsuhara, M. and Hanada, T., *An iterative search strategy for characterizing spacecraft breakup events*.

[27] Vallado, D. A., *Fundamentals of astrodynamics and applications*, volume 12, Springer Science & Business Media, 2001.

[28] Vershkov, A. N. and Grigoriev, K. V. and Kiladze, R. I. and Sochilina, A. S., *A model of distribution of geostationary satellite fragments after explosion*, 2001.